



Phosphate enhanced uranium stable immobilization on biochar supported nano zero valent iron

Yang Ruan^a, Huimin Zhang^a, Zijing Yu^a, Zenghui Diao^c, Gang Song^a, Minhua Su^a, Li'an Hou^a, Diyun Chen^a, Shuao Wang^{a,d}, Lingjun Kong^{a,b,*}

^a Guangdong Provincial Key Laboratory of Radionuclides Pollution Control and Resources, School of Environmental Science and Engineering, Guangzhou University, Guangzhou 510006, China

^b Guangdong Key Laboratory of Environmental Catalysis and Health Risk Control, School of Environmental Science and Engineering, Institute of Environmental Health and Pollution Control, Guangdong University of Technology, Guangzhou 510006, China

^c School of Environmental Science and Engineering, Zhongkai University of Agriculture and Engineering, Guangzhou 510225, China

^d School for Radiological and Interdisciplinary Sciences (RAD-X) and Collaborative Innovation Center of Medicine of Jiangsu Higher Education Institutions, Soochow University, Suzhou 215123, China

ARTICLE INFO

Editor: Dr. L. Haizhou

Keywords:

Uranium
Zero valent iron
Phosphate
Reaction sequence
Biochar

ABSTRACT

Uranium (U) immobilization from wastewater by zero valent iron (ZVI) was widely concerned through reduction and surface adsorption. Releasing of U due to re-oxidation of U(IV) into U(VI) limited the application of ZVI in U decontamination. In this work, a kind of biochar supported nano zero valent iron (Fe/BC(900)) was obtained by carbothermal reduction of starch mixed with ferric nitrate at 900 °C. U immobilization behavior by Fe/BC(900) in the presence of phosphate (P) was investigated. The U immobilization reaction was adjusted by controlling the sequence of U, Fe/BC(900) and P. U immobilization efficiency was enhanced to 99.9% in the presence of P. Reaction sequence of U, Fe/BC(900) and P influenced the U immobilization efficiency, which followed the order of (U-P)+Fe/BC(900) > (U-Fe/BC(900))+P > U+Fe/BC(900) > (P-Fe/BC(900))+U. P and nZVI both contributed to enhancing U immobilization through precipitation of uranyl-P and reductive co-precipitate (U(IV)) in a wide pH range. The released Fe ions could precipitate with uranyl and phosphate. Consumption of P and nZVI in the (P-Fe/BC(900))+U system limited U immobilization ability. The precipitate is highly dependent on U, P and Fe elements. U desorption in (U-P)+Fe/BC(900) system was not observed with stability.

1. Introduction

Uranium (U) is a rare metal widely used in nuclear fuel processing. The discharge amount of U containing wastewater is increasing with the development of nuclear fuel. U is environmentally hazardous due to its chemical toxicity and radioactivity (Tan et al., 2018). Since the U presents as soluble uranyl (UO_2^{2+}) in wastewater, it is easy to migrate in aqueous solution. Decontamination of UO_2^{2+} containing wastewater is critically necessary. Immobilization of soluble UO_2^{2+} onto solid inert medium to decrease its migration is being received a great amount of interests from researchers worldwide for U decontamination. Adsorption of UO_2^{2+} on various kinds of adsorbents such as carbonaceous (Ye et al., 2020), iron-based magnetic adsorbents (Dai et al., 2019), metal-organic framework (Feng et al., 2021), covalent organic

framework (Cui et al., 2020; S. Liu et al., 2021; X. Liu et al., 2021), phosphate (Kong et al., 2020), etc. is one of the efficient methods for UO_2^{2+} decontamination in wastewater, which is determined by the combination of UO_2^{2+} with the adsorption sites of the adsorbents (Ma et al., 2020). Thus, many works are concerned with the exploration and development of active sites for binding UO_2^{2+} .

Besides the soluble UO_2^{2+} in state of U(VI), the U performed one state of U(IV) is insoluble in aqueous solution with the advantages of low migration and easy separation. Much attention is being paid to the reduction of U(VI) into U(IV) for immobilization and extraction of UO_2^{2+} besides adsorption (S. Liu et al., 2021; X. Liu et al., 2021; Qiu et al., 2021). Until now, nano zero valent iron (nZVI) has been widely paid on environmental decontamination due to its high redox activity of -0.44 eV (Guan et al., 2015). Interestingly, reduction of U(VI) into U

* Corresponding author at: Guangdong Provincial Key Laboratory of Radionuclides Pollution Control and Resources, School of Environmental Science and Engineering, Guangzhou University, Guangzhou 510006, China.

E-mail address: kongljun@gzhu.edu.cn (L. Kong).

<https://doi.org/10.1016/j.jhazmat.2021.127119>

Received 25 May 2021; Received in revised form 26 August 2021; Accepted 1 September 2021

Available online 11 September 2021

0304-3894/© 2021 Elsevier B.V. All rights reserved.

(IV) by nZVI was also reported due to that the redox potential of $\text{UO}_2^{2+}/\text{UO}_2$ is 0.41 eV, which could be reduced by nZVI (Zhang et al., 2019). After that, remediation of UO_2^{2+} containing wastewater by nZVI was widely concerned due to the advantages of cost-effective and environment friendly. Unfortunately, nZVI tends towards agglomeration and oxidation when being exposed to the air (Phenrat et al., 2007; Ryu et al., 2011), greatly limiting its wide application in wastewater decontamination. It is promising to protect them from agglomeration and oxidation by supporting the nZVI onto porous supporters such as organic polymers (Song et al., 2021), carbonaceous materials (Jiang et al., 2021), kaolin (Lin et al., 2017), bentonite (Bao et al., 2020), zeolite (Li et al., 2020), silica (Chen et al., 2018) and alumina oxides (Ribas et al., 2019), etc. Among them, porous carbon is preferable due to its high porosity and surface area. Supporting nZVI on graphene oxide and activated carbon could be achieved by NaBH_4 reduction process, in which the graphene oxide and activated carbon were impregnated in Fe solution (Zhang et al., 2021). The adsorbed Fe ions are further reduced into nZVI being loaded on the graphene oxide and activated carbon (Goswami et al., 2020; Mandal et al., 2020). Besides NaBH_4 reduction, supporting nZVI on porous carbon also could be achieved by carbo-thermal reduction process. In this case, ferric ions are reduced into ZVI simultaneously during carbonization of organic precursors into porous carbon. A biochar supported iron adsorbent (Fe/BC) was reported in our previous work, which had considerable ability to immobilize the uranyl in wastewater by reduction and surface adsorption (Zhang et al., 2019). However, nZVI immobilized uranium is easily released into aqueous solution after being exposed to the oxidation atmosphere, performing the potential risk in long term. Immobilization of uranium with stability in long term is the key of applying nZVI for uranium immobilization.

Immobilization of uranium on hydroxyapatite was widely concerned (Kong, L. et al., 2020). Importantly, uranium immobilization on hydroxyapatite is stable in long term due to the formation of autunite, which is ascribed to the mineralization of calcium phosphate with uranyl (Morrison et al., 2021). Qiu et al. reported the co-removal of phosphate and uranium by the nZVI (Qiu et al., 2018; Zheng et al., 2020). The previous works indicated that the presence of phosphate could positively influence U removal by nZVI due to the synergistic effect of both phosphate and nZVI. The result encourages us exploring uranium immobilization by nZVI in phosphate medium. In this case, the presented phosphate is hypothesized that contributed to enhancing uranium immobilization on Fe/BC with long stability. Unfortunately, the synergistic effect of nZVI and phosphate on U removal with stability was not understood. The objective of this work is to explore the synergy effect of nZVI and phosphate on enhancing U removal. In this work, Fe/BC was conducted for U immobilization in phosphate medium. The reaction sequence among the U, nZVI, and phosphate was adjusted by controlling the adding sequence to investigate its effect on U removal characteristics. XPS and SEM-mapping analysis were conducted to confirm the reductive co-precipitate and uranyl-phosphate precipitation of uranyl with nZVI in the presence of phosphate. Besides, the phosphate removal efficiency was calculated to understand the synergy effect of nZVI and phosphate on U immobilization efficiency, further providing important information on understanding the stability of immobilized U in long term.

2. Materials and methods

2.1. Materials

Ferric Nitride ($\text{Fe}(\text{NO}_3)_3 \cdot 6\text{H}_2\text{O}$) and starch were purchased from Aladdin Bio-Chem Technology Co., Ltd (Shanghai, China). They are of analytical reagent grade. Uranyl nitrate ($\text{UO}_2(\text{NO}_3)_2 \cdot 6\text{H}_2\text{O}$) was purchased from Hubei Chushengwei Chemistry Co., Ltd in China. U(VI) stock solution in an initial concentration of 1.00 g (U)/L was prepared by dissolving 4.22 g $\text{UO}_2(\text{NO}_3)_2 \cdot 6\text{H}_2\text{O}$ into nitric acid (HNO_3) solution, further being transformed into a 1 L volumetric flask and being adjusted

to 1 L in a pH value of 3.00. The pH value in this work was adjusted by HNO_3 and sodium hydroxide (NaOH), which were purchased from Sigma-Aldrich Co., Ltd. The phosphate source in this work was tri-Potassium phosphate (K_3PO_4). They were purchased from Sigma-Aldrich Co., Ltd. The ultrapure water was used in this work.

2.2. Carbothermal reduction synthesis of Fe/BC

The Fe/BC used in this work was prepared in our previous work. The detailed method was described in the Supporting Information.

2.3. Batch adsorption and desorption process

Batch adsorption processes of U(VI) ($C_0 = 0.084 \text{ mM}$) in the absence and presence of phosphate were carried out in a series of conical flasks. The initial concentration of U(VI) was 0.084 mM. In the absence of phosphate, 0.05 g of adsorbents were poured into 50 mL U(VI) solution in a series of flasks. The flasks were placed in a digital thermostatic water bath oscillator (SHA-82A, China). The solution pH values were adjusted with 0.1 M HNO_3 and 0.1 M KOH. Each time, 5 mL of the mixture was taken out and filtered through a $0.45 \mu\text{m}$ filtration membrane to remove the suspended sorbent at the determined time interval. The residual U(VI) concentration in the filtrate was measured by a UV-Fluorescence uranium analyzer (WGJ-III, China) reported by Han et al. (2018). The adsorption capacities (q_t , mg/g) and removal efficiency (R, %) of U(VI) at “t” time could be calculated by the following equations:

$$q_t = \frac{(C_0 - C_t) \times V}{m} \quad (1)$$

$$R = \frac{C_0 - C_t}{C_0} \times 100\% \quad (2)$$

Where C_0 (mg/L) presents the initial U(VI) concentration, C_t (mg/L) and q_t (mg/g) present the residual U(VI) concentration and extraction capacity at t time (min), m (g) is the mass of the adsorbents, V (L) represents the volume of the U(VI) solution, and R (%) is the removal efficiency.

The stability of the precipitate is measured by desorption process. Desorption of the precipitate was conducted by adding Na_2CO_3 solution in oxalic condition. After extraction of U by Fe/BC(900) in the (U-Fe/BC(900))+P system, a determined volume of Na_2CO_3 solution was poured to assure the concentration of Na_2CO_3 in 1 M. After that, 5 mL of mixture was taken out and filtered through a filtration membrane to remove the suspended sorbent at the determined time interval. The residual U(VI) concentration in the filtrate was measured by a UV-Fluorescence uranium analyzer (WGJ-III, China).

2.4. Analytical methods

The X-ray diffraction (XRD) patterns were measured with Cu K α at 40 kV and 40 mA in the range of 5–80° by using a powder X-ray diffractometer (PW3040/60, PANalytical, Holland). The surface morphology and mapping analysis were both conducted by a scanning electron microscope (SEM) (JED-2300, JEOL, Japan). The X-ray photoelectron spectroscopy (XPS) spectra were measured using an electron spectrometer (Thermo Escalab 250).

3. Results and discussion

3.1. Phosphate enhanced U immobilization

Our previous work reported that the carbonization temperature influenced the formation of nZVI, which is shown in Fig. S1. nZVI in nanosphere was formed for Fe/BC(900) once the temperature increased to 900 °C. Fe/BC(900) had favorable ability for extracting uranium, but uranium release was founded when the U and nZVI were exposed to the oxidation atmosphere, resulting in the risk of U leaching. Uranium

mineralization with hydroxyapatite was founded in our previous study due to precipitation. The dissolved phosphate played an important role in forming autunite (Kong et al., 2020). Co-removal of uranium and phosphate by nZVI was reported by Zheng et al. (2020). The effect of phosphate on the enhanced uranium removal efficiency by Fe/BC(900) was investigated. It was well known that the uranium species is pH dependent, also the dissolution rate and redox potential of uranyl nitrate is changed as shown in Fig. S2. The uranium immobilization efficiencies as a function of pH value was presented in Fig. 1, in which the Fe/BC(900) dosage was 1 g/L, and the uranium initial concentration was 0.168 mM. In this case, phosphate was firstly added into the uranium solution, after that Fe/BC(900) was added in the mixed solution, which was named as (U-P)+Fe/BC(900) system. Among them, the molar ratio of U to P is controlled in 1:1, 1:2, and 2:1 in the (U-P)+Fe/BC(900) system, they are marked as (U-P = 1:1)+Fe/BC(900), (U-P = 1:2)+Fe/BC(900) and (U-P = 2:1)+Fe/BC(900), respectively. In the absence of phosphate, the uranium removal efficiency by Fe/BC(900) in the (U-P)+Fe/BC(900) systems was improved with the increase in the pH value, which achieved to the highest efficiency of 94.3% when the pH value was 6. The low removal efficiency of uranium at the acidic solution is ascribed to the competitive reaction between H^+ and uranium. In this system, Fe^{2+} and Fe^{3+} are released into the acidic solution. Besides, the Fe/BC(900) surface is positive charged when the pH value is lower than 6.81 due to the pH_{zpc} of Fe/BC(900) was 6.81. The electrostatic repulsion decreased as the pH value increased to 6.81, leading to the increase in the uranium removal efficiency. Interestingly, the uranium removal efficiency is enhanced in the presence of phosphate. The uranium performs in the form of UO_2HPO_4 in the pH value of 4–8 due to the presence of phosphate, while it performs UO_2^{2+} when the pH value is lower than 4 as shown in Fig. 1. In this case, the uranium is positive and neutral charged in the pH value of 2–4 and 4–8, respectively. The increase in the uranium removal efficiencies as a function of pH value from 2 to 5 is due to the change of uranium species from UO_2^{2+} to UO_2HPO_4 , in which the electronic repulsion between the Fe/BC(900) and uranium is decreased, which also favors the uranium reduction by nZVI. As the pH value increased to 6, the uranium removal efficiency decreased. It is due to the negative charged Fe/BC(900), which is not favorable for the adsorption of UO_2HPO_4 . In this case, the uranium removal is only ascribed to the ZVI reduction. The results indicate that the addition of phosphate could enhance the uranium removal efficiency at the pH value ranging from 4 to 6. Interestingly, uranium removal efficiencies were enhanced by increasing the molar ratio of P and U to 1:1 and 2:1 for the (P-U=1:1)+Fe/BC(900) and (P-U=2:1)+Fe/BC(900) systems, in

which the amount of phosphate was increased. Enough uranium is favorable for uranium immobilization by electrostatic attraction. Besides, the released Fe ions could precipitate with $UO_2(PO_4)_2^{2-}$, contributing to the uranium immobilization. Thus, the uranium immobilization is enhanced in the (P-U=2:1)+Fe/BC(900) system. When the pH value is 2–3, UO_2^{2+} is the main phase. Only ZVI reduction contributed to uranium immobilization. The electrostatic repulsion leads to unfavorable uranium removal efficiency. The released Fe^{2+} could react with UO_2^{2+} in the presence of phosphate to form the precipitate, resulting in enhanced uranium removal efficiency. When the pH value was 8–9, the uranium removal efficiencies decreased. In this case, the uranium existed in the form of $UO_2(PO_4)_2^{2-}$ with the company of phosphate. It means that the phosphate presented could not favor the uranium immobilization due to the electronic repulsion between $UO_2(PO_4)_2^{2-}$ and Fe/BC(900) in the basic solution. The enhanced uranium removal efficiencies in the presence of phosphate are ascribed to the formation of UO_2HPO_4 in acidic solution.

3.2. Phosphate enhanced uranium immobilization mechanism

To further confirm the enhanced uranium removal mechanism in the presence of phosphate, the reaction sequence of the UO_2^{2+} , PO_4^{3-} , and Fe/BC(900) were controlled to adjust the uranium reaction process. Fig. 2 presents the uranium removal efficiencies in different additional orders, which were named as (P-Fe/BC(900))+U, (U-Fe/BC(900))+P, and (P-U)+Fe/BC(900) systems according to the adding sequence of uranyl, phosphate solution, and Fe/BC(900). In the (P-Fe/BC(900))+U system, although the phosphate is presented in a U/P molar ratio of 1:2, uranium removal efficiencies are highly inhibited, especially in the pH value of 3–7. Since the phosphate could be removed by nZVI through forming $Fe_3(PO_4)_2$ and $FePO_4$ precipitates (Xie et al., 2014), phosphate and nZVI were consumed firstly in the (P-Fe/BC(900))+U system. Consumption of nZVI and P resulted in the competition of uranium. Thus, the uranium removal efficiencies were greatly decreased compared to those in (U-Fe/BC(900))+P and (U-P)+Fe/BC(900) systems as shown in Fig. 3(a). It confirms that the reaction of nZVI and P inhibited U immobilization even in the presence of P. Conversely, phosphate removal efficiencies are higher than 90% (Fig. 3b), indicating that the added phosphate could contribute to enhancing uranium removal, but phosphate could consume nZVI in (P-Fe/BC(900))+U system, which leads to the competition of uranium. Thus, the uranium removal efficiency in the (P-Fe/BC(900))+U system was lower than those in the U+Fe/BC(900) system. Considering the (U-Fe/BC(900))+P

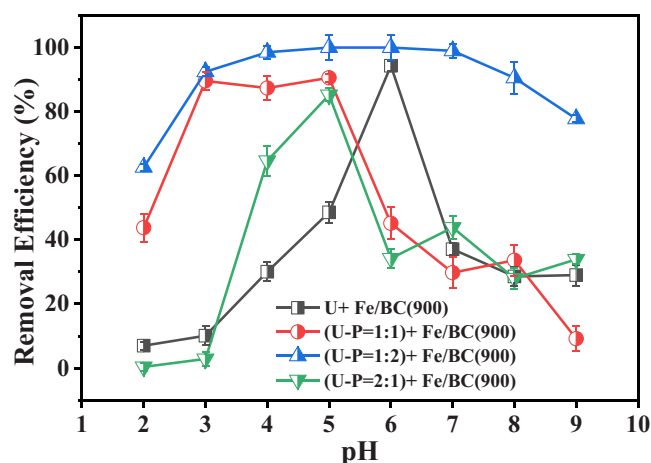


Fig. 1. The change in the U removal efficiency as a function of pH value in U+Fe/BC(900) system and (U-P)+Fe/BC(900) system in different molar ratio of U/P (C(U) = 0.168 mM, dosage(Fe/BC(900)) = 1 g/L) (The (U-P = 1:1)+Fe/BC(900), (U-P = 1:2)+Fe/BC(900) and (U-P = 2:1)+Fe/BC(900) systems indicated that the molar ratio of U to P is 1:1, 1:2 and 2:1, respectively.).

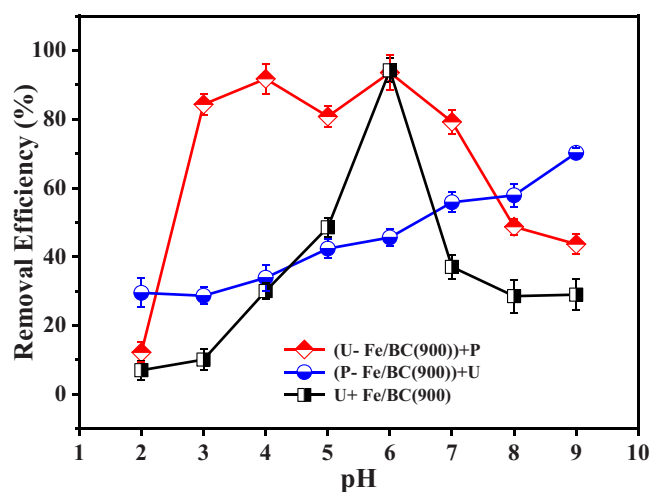


Fig. 2. The effect of addition sequences of phosphate on the removal efficiencies of U(VI) by Fe/BC(900) (C(U) = 0.168 mM, dosage = 1 g/L, U:P = 1:2).

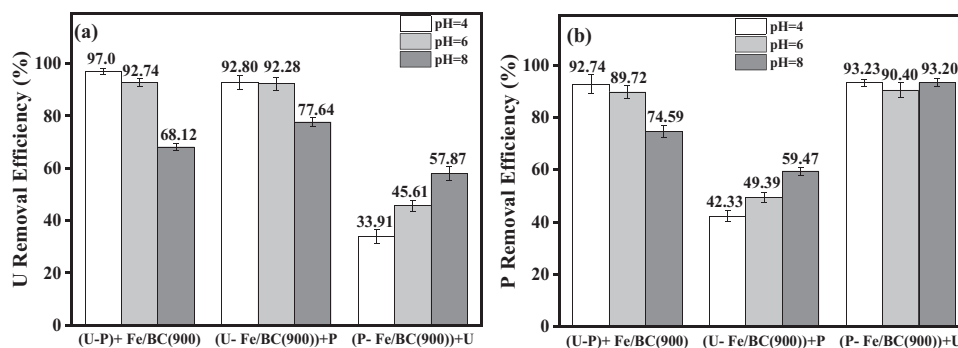


Fig. 3. Removal efficiency of (a) U(VI) and (b) P by Fe/BC(900) with different addition sequences of phosphate at different pH ($C(U) = 0.168$ mM, $T = 25$ °C, dosage = 1 g/L, U:P = 1:2).

system, the U removal efficiencies could be enhanced after the addition of phosphate compared that in U+Fe/BC(900) system. As being described in the (U-Fe/BC(900))+P system, ZVI reduction contributed to U immobilization. Although the Fe ions are released when the pH value in solution is lower than 7, the added phosphate could react with UO_2^{2+} and released Fe^{2+}/Fe^{3+} to form precipitate. In this case, the U immobilization efficiency was favorable. However, only 42.33% and 59.47% of phosphate are removed in the pH value of 4–8 in the (U-Fe/BC(900))+P system (Fig. 3), suggesting that U is immobilized by ZVI reduction and the residual U could react with parts of phosphate. The unfavorable P removal efficiency is consistent with the results of ZVI reduction of uranium. While considering for the (U-P)+Fe/BC(900) system, the molar ratio of U and P is 1:2, the uranium and phosphate could react adequately, further being immobilized by the addition of Fe/BC(900). Thus, the U and P removal efficiencies were both higher than 90% in the tested pH range. The above results indicated that the reaction of added P with Fe/BC(900) before U addition is unfavorable for P and U immobilization, while the formation of U and P favored its immobilization by Fe/BC(900).

To further elucidate the enhanced effect of P on U immobilization efficiency, the phosphate concentration increased from 0.168 to 0.672 mM. The P and U removal efficiencies as a function of increased P concentration in the (P-Fe/BC(900))-U and P+Fe/BC(900) systems are presented in Fig. 4. It is shown in Fig. 4. (a) that 92.59% of P was removed in the P+Fe/BC(900) system when the initial P concentration is 0.168 mM, confirming that the Fe/BC(900) could consume the phosphate. Thus, the consumption of P by Fe/BC(900) resulted in unfavorable U removal efficiency as being described above. Besides, the phosphate removal efficiency decreased with the increase in phosphate concentration in the P+Fe/BC(900) system, indicating that the residual P concentration increased as the increased initial phosphate concentration, while the phosphate removal efficiencies were about 97.16% and 98.10% in the (P-Fe/BC(900))+U system in the presence of

uranium. The uranium immobilization capacity is equal to about 19.98 mg/g once the dosage of Fe/BC(900) is 1 g/L. Comparing to the uranium adsorption capacity by the Fe/Mn binary oxide in a dosage of 1 g/L (Du et al., 2016), the Fe/BC(900) has favorable ability to adsorb uranium due to the reduction property of zero valent iron. The results indicated that the addition of uranium could react with the residual phosphate, which is consistent with the aforementioned result of the formation of U-P precipitate. Fortunately, the uranium removal efficiency increased with the increase in phosphate concentration, further confirming that the excess phosphate enhanced uranium immobilization. The formation of U-P precipitate greatly influenced the uranium immobilization by Fe/BC(900).

The kinetics of uranium extraction at different temperatures in the (U-P)+Fe/BC(900) system are presented in Fig. 5 to elucidate the uranium immobilization process. It is shown that uranium immobilization is time-dependent. At the temperature of 25 °C, uranium immobilization efficiency achieved equilibrium at about 40 min. Once the temperature increased to 35 and 45 °C, uranium immobilization efficiencies achieved equilibrium within 20 min even to 10 min, suggesting that the temperature speeded the uranium immobilization rate. Pseudo-first-order and Pseudo-second-order kinetic models were conducted to evaluate the kinetic parameters, which were shown in Table 1. It can be seen from Table 1 that the pseudo-first-order kinetic model fitted well to the uranium extraction results according to the correlation efficiency. Extraction kinetic rate of Fe/BC(900) to uranium at 45 °C is 1.079 min^{-1} , which is higher than those in 25 and 35 °C. It is well-known that the increased temperature could accelerate the molecule transformation. Then the immobilization rate is enhanced at the temperature of 45 °C comparing to that at 25 °C. Thus, the immobilization rate of uranium in the (U-P)+Fe/BC(900) system is temperature-dependent being ascribed to the ZVI reduction and precipitation of Fe ions with $UO_2(PO_4)_2$.

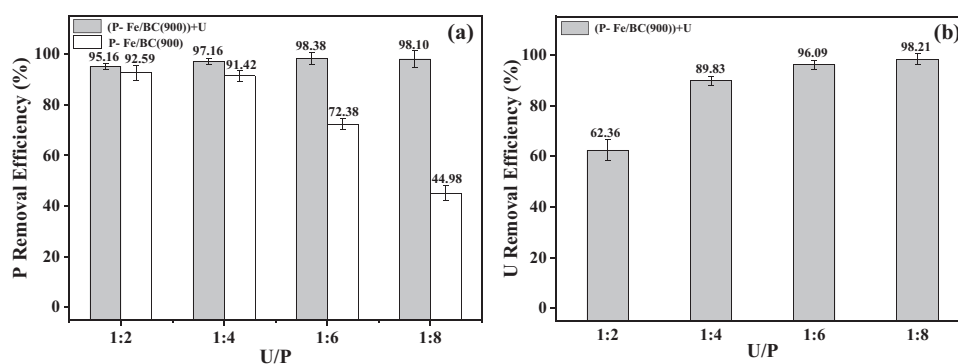


Fig. 4. Removal efficiencies of (a) P and (b) U(VI) with different molar ratio of U to P in (P-Fe/BC(900))+U system ($C(U) = 0.168$ mM, $T = 25$ °C, dosage = 1 g/L, pH = 4).

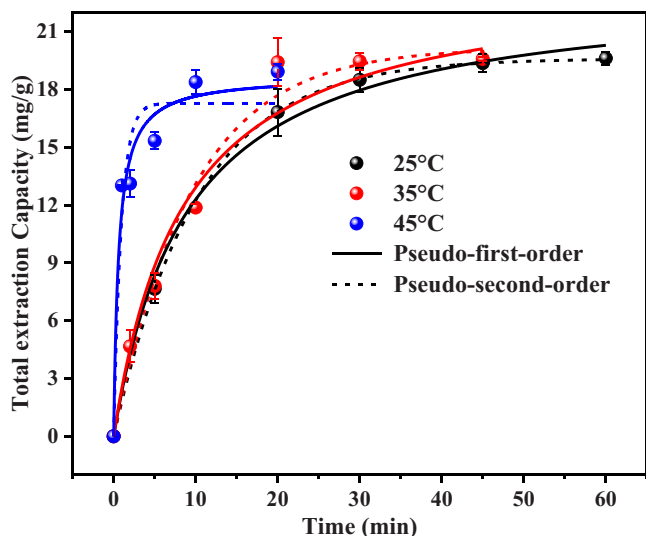


Fig. 5. The pseudo-first-order and pseudo-second-order kinetic models of uranium extracted by Fe/BC(900) in (U-P)+Fe/BC(900) system at 25, 35 and 45 °C, pH= 4.

3.3. Uranium immobilization fate and stability

The uranium fate in the (U-P)+Fe/BC(900), (P-Fe/BC(900))+U, and (U-Fe/BC(900))+P systems was investigated by XPS, XRD, and SEM

analysis. Fig. S3 presents the full-range XPS survey spectra of Fe/BC(900) after adsorption of uranium in phosphate medium for (P-Fe/BC(900))+U, (U-P)+Fe/BC(900), and (U-Fe/BC(900))+P systems. The major elements of carbon, oxygen, iron, uranium, and phosphorus were all observed. The presence of uranium and phosphorus indicated that uranium and phosphorus are both captured on the Fe/BC(900) surface. The narrow XPS spectra of Fe 2p and U 4f for (P-Fe/BC(900))+U, (U-P)+Fe/BC(900), and (U-Fe/BC(900))+P systems were shown in Fig. 6 (a) and (b). Obviously, the high-resolution Fe 2p XPS spectra can be deconvoluted into three peaks, which are assigned to Fe(0), Fe(II), and Fe(III). The presented Fe(II) and Fe(III) indicated the coexisted Fe(II)/Fe(III) oxides, suggesting the oxidation of ZVI by UO_2^{2+} . The results are consistent with the results reported by Zheng, H. et al. (2020). Another peak being assigned to Fe(0) is also observed, which is also obtained from the XRD analysis as shown in Fig. S4. It is ascribed to the residual ZVI in the core after reduction with UO_2^{2+} . Obviously, the peak intensity of Fe(0) was weakened after the reaction of Fe(0) with UO_2^{2+} , confirming that the Fe(0) is involved in the reduction of UO_2^{2+} . The Fe(0) was converted into iron oxides as shown in Fig. 6. It can also be confirmed by the high-resolution U 4f XPS spectra that were deconvoluted into two peaks being assigned to U(VI) and U(IV). The formed U(IV) may result from the reduction of U(VI) into U(IV). Although the phosphate was involved in uranyl removal, the precipitate crystal was not founded according to the XRD analysis. It may be due to the amorphous precipitate of uranium. SEM-mapping analysis of precipitate formed in (U-P)+Fe/BC(900), (U-Fe/BC(900))+P, and (P-Fe/BC(900))+U systems were conducted in Fig. 7(a), (b), and (c), respectively. Obviously, nano-flake was observed on the surface of precipitates. It was

Table 1

Nonlinear fitted pseudo-first-order and pseudo-second-order models of U(VI) extraction by Fe/BC(900) in (U-P)+Fe/BC(900) system at 25, 35 and 45 °C.

Temperature	Pseudo-first-order			Pseudo-second-order		
	k_1 (min^{-1})	q_e (mg/g)	R^2	k_2 ($\text{g}/(\text{mg min})$)	q_e (mg/g)	R^2
25 °C	0.0981	19.60	0.9999	4.783×10^{-3}	23.32	0.9645
35 °C	0.1049	20.16	0.9868	4.902×10^{-3}	23.93	0.9732
45 °C	1.079	17.28	0.9383	8.998×10^{-2}	18.70	0.9733

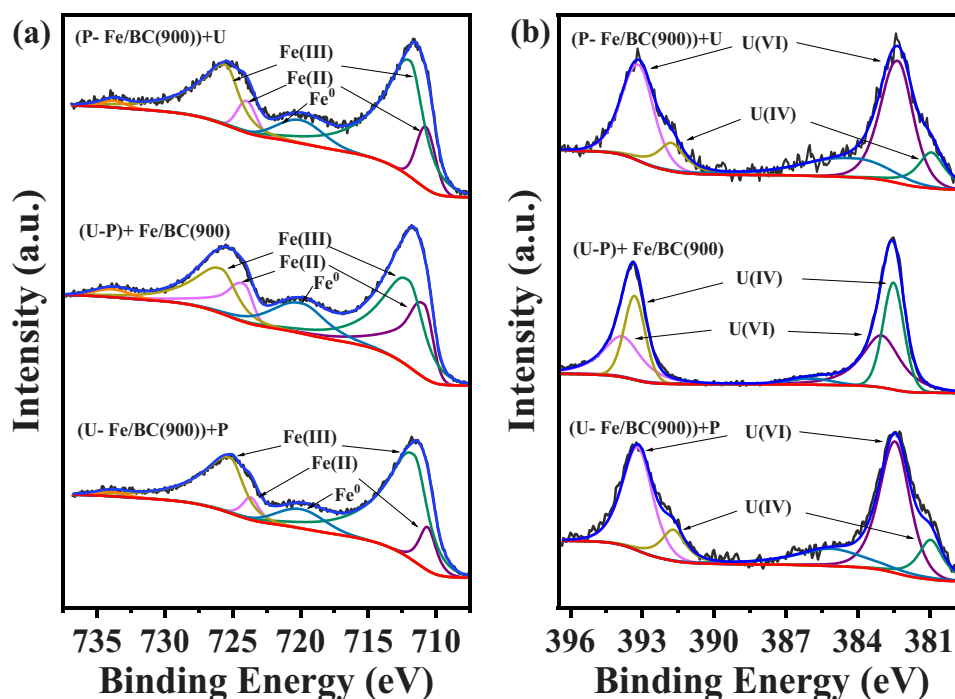


Fig. 6. The narrow XPS spectra of (a) Fe 2p and (b) U 4f for (P-Fe/BC(900))+U, (U-P)+Fe/BC(900) and (U-Fe/BC(900))+P.

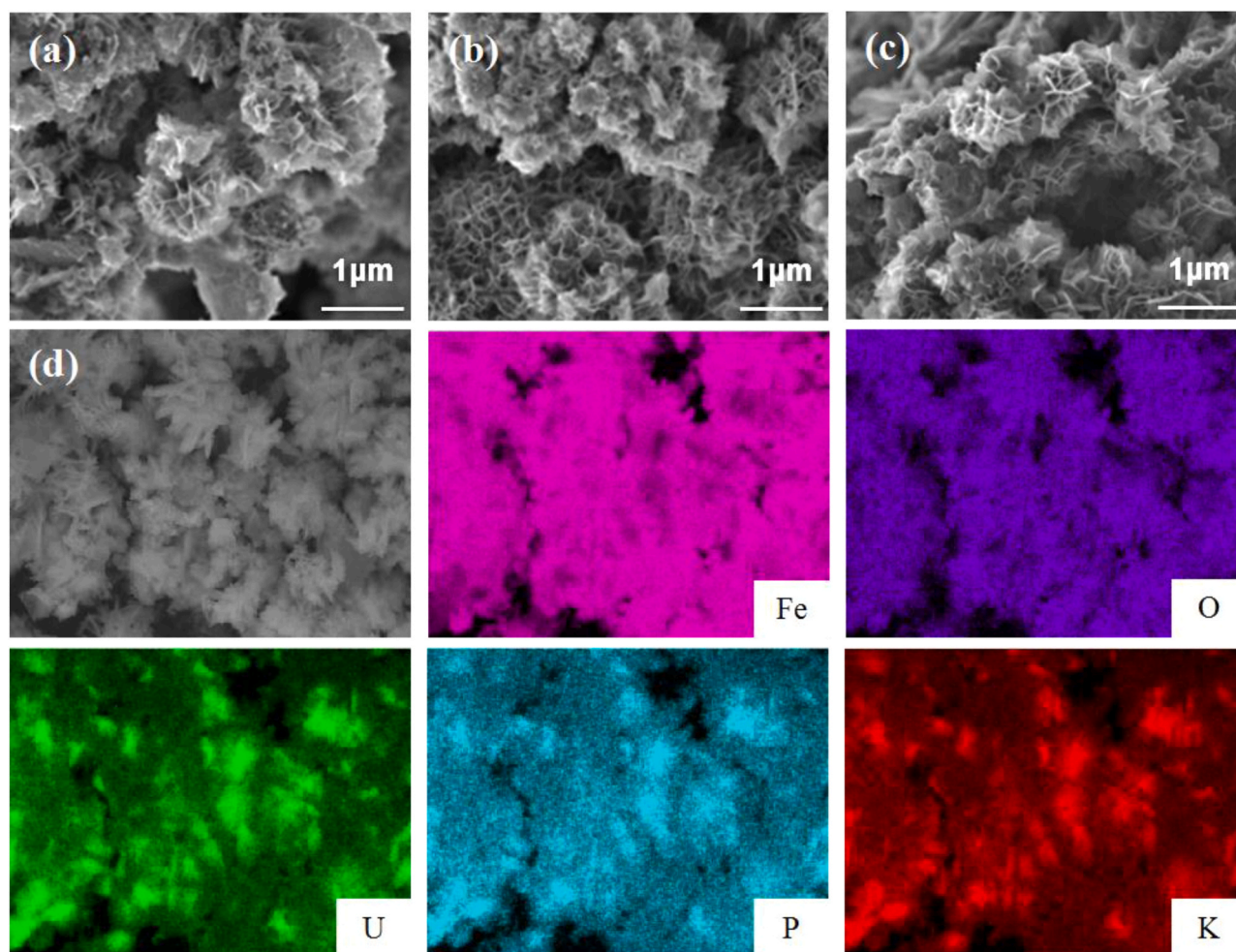


Fig. 7. SEM images of the precipitate obtained at (a) (U-P)+Fe/BC(900); (b) (U-Fe/BC(900))+P; (c) (P-Fe/BC(900))+U and (d) SEM-mapping of (U-P)+Fe/BC(900).

different from the morphology obtained from our previous work, in which the uranium was immobilized by nZVI in the absence of phosphate (Zhang et al., 2019). They were consistent with the micromorphology of autunite formed by the reaction of uranyl with phosphate as reported in our previous study (Han et al., 2018). However, the micromorphology is significantly different from that obtained from uranyl immobilization by Fe/BC(900) in our previous work (Zhang et al., 2019). The result confirmed that the phosphate involved the removal of uranyl by forming autunite miner. SEM-mapping of precipitate form in (U-P)+Fe/BC(900) system as shown in Fig. 7(d) confirmed the presence of P, U, Fe element. Distribution of U is dependent on the mapping of Fe and P elements, further confirming the coexisted of U, Fe, and P for the fate of precipitate.

The stability of precipitate is very important for uranium immobilization, which is determined by the desorption behavior of uranium. To investigate the desorption of uranium from precipitates in the (U-Fe/BC(900))+P system under the condition of molar ratio U:P:Fe = 1:2:6 and 1:2:8, 1 M Na_2CO_3 was added into the solution after the complete reaction of U for 40 h due to the fact that both U(VI) and U(IV) are soluble in concentrated Na_2CO_3 (Noubactep et al., 2003). It can be seen from Fig. 8 that little uranium was released in 1 M Na_2CO_3 solution. The uranium desorption efficiency is about 17%. Du et al. (2016) reported that uranium desorption efficiency from Fe-Mn binary oxide was high to 64%, while uranium desorption efficiency from uraninite is about 10% in a reduction atmosphere (Jung et al., 2012). Uranium desorption in this work was the lowest that could be neglected in the presence of phosphate. It may be due to the formation of phosphuranylite minerals

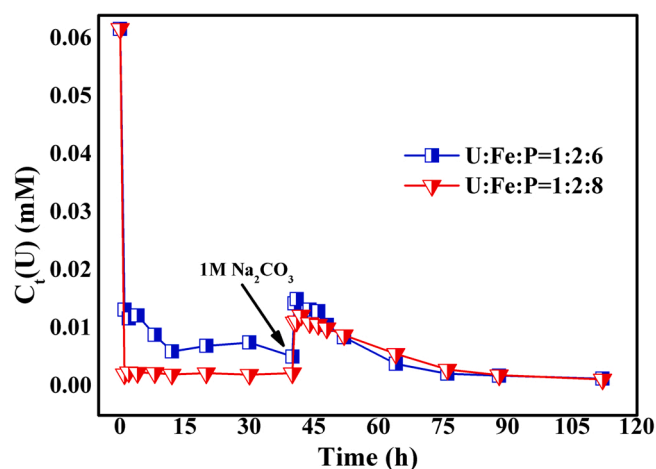


Fig. 8. The change of uranium in (U-Fe/BC(900))+P systems and uranium desorption in the presence of Na_2CO_3 .

in the presence of phosphate. Thus, uranium immobilization by Fe/BC(900) in the presence of phosphate performed stability in the long term, which can be ascribed to the mineralization of uranyl, ZVI, and phosphate. nZVI reduction and precipitation both contributed to uranium immobilization. The reaction process and characterization of the precipitate will be investigated in our further work to understand the fate of

uranium in the (U-P)+Fe/BC(900) system.

4. Conclusion

The presence of phosphate was involved in uranium immobilization on Fe/BC(900). Reaction sequence influenced uranium immobilization by Fe/BC(900). The removal ability of Fe/BC(900) for U(VI) decreases in the order of (U-P)+Fe/BC(900), (U-Fe/BC(900))+P, U+Fe/BC(900), (P-Fe/BC(900))+U. (U-P)+Fe/BC(900) system had favorable uranium immobilization ability through the formation of P-U complexes. The released Fe ions could precipitate with uranyl and phosphate, leading to enhanced uranium immobilization in a wide pH range. Consumption of P and Fe in the (P-Fe/BC(900))+U system limited uranium immobilization ability, confirming the involved reaction of P and Fe for uranium immobilization. nZVI reduction and precipitation both contributed to uranium immobilization. The precipitate is highly dependent on U, P and Fe elements. Desorption of uranium in (U-P)+Fe/BC(900) system was neglected due to the formation of the phosphate-uranium precipitate.

CRediT authorship contribution statement

Lingjun Kong*: Conceptualization, Supervision. **Yang Ruan**: Methodology, Writing – original draft preparation. **Huimin Zhang**: Conducting experiment. **Zijing Yu**: Data analysis, Water chemistry analysis. **Zenghui Diao**: Writing – review & editing. **Gang Song**: Uranium concentration analysis. **Minhua Su**: XRD analysis. **Li'an Hou**: Conceptualization. **Diyun Chen**: Writing – review & editing. **Shuao Wang**: Writing – review & editing.

Declaration of Competing Interest

The authors declare that they have no known competing financial interests or personal relationships that could have appeared to influence the work reported in this paper.

Acknowledgments

This work was supported by the National Natural Science Foundation of China (21976042), The National Key Research and Development Program of China (No. 2019YFC1904101, 2019YFC1904102), the Project of Guangdong Provincial Key Laboratory of Radioactive Contamination Control and Resources (2017B030314182), Guangdong Key Laboratory of Environmental Catalysis and Health Risk Control (2018B030322014), Guangdong Basic and Applied Basic Research Foundation (2019A1515011543), Science and Technology Planning Project of Guangdong Province, China (2021A0505030076), Guangdong Province Universities and Colleges Pearl River Scholar Funded Scheme (2018, 2019), University Scientific Research Project of Guangzhou Education Bureau (201831803), the research project of Guangzhou University (YK2020012).

Appendix A. Supporting information

Supplementary data associated with this article can be found in the online version at [doi:10.1016/j.jhazmat.2021.127119](https://doi.org/10.1016/j.jhazmat.2021.127119).

References

- Bao, T., Dantie, M.M., Hosseinzadeh, A., Wei, W., Jin, J., Vo, H.N.P., Ye, J.S., Liu, Y., Wang, X.F., Yu, Z.M., 2020. Bentonite-supported nano zero-valent iron composite as a green catalyst for bisphenol A degradation: Preparation, performance, and mechanism of action. *J. Environ. Manag.* 260, 110105.
- Chen, S., Belver, C., Li, H., Ren, L.Y., Liu, Y.D., Bedia, J., Gao, G.L., Guan, J., 2018. Effects of pH value and calcium hardness on the removal of 1,1,1-trichloroethane by immobilized nanoscale zero-valent iron on silica based supports. *Chemosphere* 211, 102–111.

- Cui, W., Zhang, C., Jiang, W., Li, F., Liang, R., Liu, J., Qiu, J., 2020. Regenerable and stable sp² carbon-conjugated covalent organic frameworks for selective detection and extraction of uranium. *Nat. Commun.* 11 (1), 436.
- Dai, S., Wang, N., Qi, C., Wang, X., Ma, Y., Yang, L., Liu, X., Huang, Q., Nie, C., Hu, B., Wang, X., 2019. Preparation of core-shell structure Fe₃O₄@C@MnO₂ nanoparticles for efficient elimination of U(VI) and Eu(III) ions. *Sci. Total Environ.* 685, 986–996.
- Du, L., An, S., Ding, J., Jiang, D., Hong, W., Jin, Y., Liu, L., Wang, R., Zhang, D., Xia, C., 2016. Adsorption and desorption of uranium(VI) by Fe-Mn binary oxide in aqueous solutions. *J. Radioanal. Nucl. Chem.* 308 (2), 545–554.
- Feng, L., Wang, H., Feng, T., Yan, B., Yu, Q., Zhang, J., Guo, Z., Yuan, Y., Ma, C., Liu, T., Wang, N., 2021. In-situ synthesis of uranyl-imprinted nanocage for selective uranium recovery from seawater. *Angew. Chem. Int. Ed. Engl.* <https://doi.org/10.1002/ange.202101015>.
- Goswami, A., Kadam, R.G., Tucek, J., Sofer, Z., Bousa, D., Varma, R.S., Gawande, M.B., Zboril, R., 2020. Fe(0)-embedded thermally reduced graphene oxide as efficient nanocatalyst for reduction of nitro compounds to amines. *Chem. Eng. J.* 382, 122469.
- Guan, X., Sun, Y., Qin, H., Li, J., Lo, I.M.C., He, D., Dong, H., 2015. The limitations of applying zero-valent iron technology in contaminants sequestration and the corresponding countermeasures: the development in zero-valent iron technology in the last two decades (1994–2014). *Water Res.* 75, 224–248.
- Han, M., Kong, L., Hu, X., Chen, D., Xiong, X., Zhang, H., Su, M., Diao, Z., Ruan, Y., 2018. Phase migration and transformation of uranium in mineralized immobilization by wasted bio-hydroxyapatite. *J. Clean. Prod.* 197, 886–894.
- Jiang, Q., Zhang, Y., Jiang, S., Wang, Y., Li, H., Han, W., Qu, J., Wang, L., Hu, Y., 2021. Graphene-like carbon sheet-supported nZVI for efficient atrazine oxidation degradation by persulfate activation. *Chem. Eng. J.* 403, 126309.
- Jung, H.B., Boyanov, M.I., Konishi, H., Sun, Y., Mishra, B., Kemner, K.M., Roden, E.E., Xu, H., 2012. Redox behavior of uranium at the nanoporous aluminum oxide-water interface: implications for uranium remediation. *Environ. Sci. Technol.* 46 (13), 7301–7309.
- Kong, L., Ruan, Y., Zheng, Q., Su, M., Diao, Z., Chen, D., Hou, L., Chang, X., Shih, K., 2020. Uranium extraction using hydroxyapatite recovered from phosphorus containing wastewater. *J. Hazard. Mater.* 382, 120784.
- Li, Z., Wang, L., Wu, J., Xu, Y., Wang, F., Tang, X., Xu, J., Ok, Y.S., Meng, J., Liu, X., 2020. Zeolite-supported nanoscale zero-valent iron for immobilization of cadmium, lead, and arsenic in farmland soils: encapsulation mechanisms and indigenous microbial responses. *Environ. Pollut.* 260, 114098.
- Lin, J., Sun, M., Liu, X., Chen, Z., 2017. Functional kaolin supported nanoscale zero-valent iron as a Fenton-like catalyst for the degradation of Direct Black G. *Chemosphere* 184, 664–672.
- Liu, S., Wang, Z., Lu, Y., Li, H., Chen, X., Wei, G., Wu, T., Maguire, D.-J., Ye, G., Chen, J., 2021a. Sunlight-induced uranium extraction with triazine-based carbon nitride as both photocatalyst and adsorbent. *Appl. Catal. B: Environ.* 282, 119523.
- Liu, X., Pang, H., Liu, X., Li, Q., Zhang, N., Mao, L., Qiu, M., Hu, B., Yang, H., Wang, X., 2021b. Orderly porous covalent organic frameworks-based materials: superior adsorbents for pollutants removal from aqueous solutions. *Innovation* 2 (1), 100076.
- Ma, F., Gui, Y., Liu, P., Xue, Y., Song, W., 2020. Functional fibrous materials-based adsorbents for uranium adsorption and environmental remediation. *Chem. Eng. J.* 390, 124597.
- Mandal, S., Pu, S., He, L., Ma, H., Hou, D., 2020. Biochar induced modification of graphene oxide & nZVI and its impact on immobilization of toxic copper in soil. *Environ. Pollut.* 259, 113851.
- Morrison, K.D., Zavarin, M., Kersting, A.B., Begg, J.D., Mason, H.E., Balboni, E., Jiao, Y., 2021. Influence of uranium concentration and pH on U-phosphate biomineralization by *Caulobacter* OR37. *Environ. Sci. Technol.* 55 (3), 1626–1636.
- Noubactep, C., Meinrath, G., Dietrich, P., Merkel, B., 2003. Mitigating uranium in groundwater: prospects and limitations. *Environ. Sci. Technol.* 37 (18), 4304–4308.
- Phenrat, T., Saleh, N., Sirk, K., Tilton, R.D., Lowry, G.V., 2007. Aggregation and sedimentation of aqueous nanoscale zerovalent iron dispersions. *Environ. Sci. Technol.* 41 (1), 284–290.
- Qiu, M., Liu, Z., Wang, S., Hu, B., 2021. The photocatalytic reduction of U(VI) into U(IV) by ZIF-8/g-C₃N₄ composites at visible light. *Environ. Res.* 196, 110349.
- Qiu, M., Wang, M., Zhao, Q., Hu, B., Zhu, Y., 2018. XANES and EXAFS investigation of uranium incorporation on nZVI in the presence of phosphate. *Chemosphere* 201, 764–771.
- Ribas, D., Peskova, K., Jubany, I., Parma, P., Cernik, M., Benito, J.A., Marti, V., 2019. High reactive nano zero-valent iron produced via wet milling through abrasion by alumina. *Chem. Eng. J.* 366, 235–245.
- Ryu, A., Jeong, S.-W., Jang, A., Choi, H., 2011. Reduction of highly concentrated nitrate using nanoscale zero-valent iron: effects of aggregation and catalyst on reactivity. *Appl. Catal. B: Environ.* 105 (1–2), 128–135.
- Song, Y., Zeng, Y., Liao, J., Chen, J., Du, Q., 2021. Efficient removal of sulfamethoxazole by resin-supported zero-valent iron composites with tunable structure: performance, mechanisms, and degradation pathways. *Chemosphere* 269, 128684.
- Tan, X., Fang, M., Tan, L., Liu, H., Ye, X., Hayat, T., Wang, X., 2018. Core-shell hierarchical C@Na₂Ti₃O₇ center dot 9H₂O nanostructures for the efficient removal of radionuclides. *Environ. Sci. Nano* 5 (5), 1140–1149.
- Xie, B., Zuo, J., Gan, L., Liu, F., Wang, K., 2014. Cation exchange resin supported nanoscale zero-valent iron for removal of phosphorus in rainwater runoff. *Front. Environ. Sci. Eng.* 8 (3), 463–470.
- Ye, T., Huang, B., Wang, Y., Zhou, L., Liu, Z., 2020. Rapid removal of uranium (VI) using functionalized luffa rattan biochar from aqueous solution. *Colloids Surf. A: Physicochem. Eng. Asp.* 606, 125480.
- Zhang, H., Ruan, Y., Liang, A., Shih, K., Diao, Z., Su, M., Hou, L., Chen, D., Lu, H., Kong, L., 2019. Carbothermal reduction for preparing nZVI/BC to extract uranium:

- insight into the iron species dependent uranium adsorption behavior. *J. Clean. Prod.* 239, 117873.
- Zhang, Q., Wang, Y., Wang, Z., Zhang, Z., Wang, X., Yang, Z., 2021. Active biochar support nano zero-valent iron for efficient removal of U(VI) from sewage water. *J. Alloy. Compd.* 852, 156993.
- Zheng, H., Ren, X., Zhang, X., Song, G., Chen, D., Chen, C., 2020. Mutual effect of U(VI) and phosphate on the reactivity of nanoscale zero-valent iron (nZVI) for their co-removal. *J. Mol. Liq.* 297, 111853.